Topology-Guided Design and Syntheses of Highly Stable Mesoporous Porphyrinic Zirconium Metal−Organic Frameworks with High Surface Area

Tian-Fu Liu,[†,§] Dawei Feng,[†,§] Ying-Pin Chen,[†,‡] Lanfang Zou,[†] Mathieu Bosch,[†] Shuai Yuan,[†] Zhangwen Wei,[†] Stephen Fordham,[†] Kecheng Wang,[†] and Hong-Cai Zhou*,[†]

[†]Department of Chemistry, Texas A&M University, College Station, Texas 77842-3012, United States
[‡]Department of Material Science and Engineering, Texas A&M University, College Station, Texas 77843, United States

S Supporting Information

ABSTRACT: Through a topology-guided strategy, a series of Zr_6-containing isoreticular porphyrinic metal−organic frameworks (MOFs), **PCN-228**, **PCN-229**, and **PCN-230**, with **ftw-a** topology were synthesized using the extended porphyrinic linkers. The bulky porphyrin ring ligand effectively prevents the network interpenetration which often appears in MOFs with increased linker length. The pore apertures of the structures range from 2.5 to 3.8 nm, and **PCN-229** demonstrates the highest porosity and BET surface area among the previously reported Zr-MOFs. Additionally, by changing the relative direction of the terminal phenyl rings, this series replaces a Zr_8 cluster with a smaller Zr_6 cluster in a topologically identical framework. The high connectivity of the Zr_6 cluster yields frameworks with enhanced stability despite high porosity and ultralarge linker. As a representative example, **PCN-230**, constructed with the most extended porphyrinic linker, shows excellent stability in aqueous solutions with pH values ranging from 0 to 12 and demonstrates one of the highest pH tolerances among all porphyrinic MOFs. This work not only presents a successful example of rational design of MOFs with desired topology, but also provides a strategy for construction of stable mesoporous MOFs.
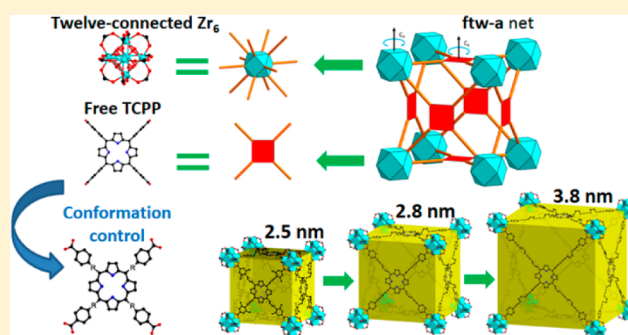
■ INTRODUCTION

Mesoporous metal−organic frameworks (MOFs) have attracted great interest as heterogeneous platforms to immobilize or encapsulate functional moieties, such as organometallic catalysts, nanoparticles, and enzymes.[1,2] However, compared with the well-explored microporous MOFs, mesoporous MOFs are relatively under-developed. This is ascribed to the difficulty in organic linker extension, challenges in activation of MOFs with ultralarge pores, as well as the common appearance of undesired interpenetration.[2b,3] Moreover, the stability of the framework becomes difficult to maintain after extension of the organic linker, especially for mesoporous materials whose applications are usually conducted under aqueous or harsh chemical environments. The majority of reported carboxylate containing MOFs are constructed with relatively soft Lewis acidic metal species, such as Cu^{2+} and Zn^{2+}. The weak coordination bond between the soft Lewis acid and hard Lewis base causes their low stability and severely hampers further exploration of their potential.[4] To improve the chemical stability of MOFs, hard Lewis acidic species such as Al^{3+}, Fe^{3+}, Cr^{3+}, and Zr^{4+}, which can form much stronger bonds with carboxylates, are often incorporated.[5,6] Despite this adjustment, as isoreticular chemistry is applied to augment the internal

cavity of known MOF structures, the pore size and stability are usually inversely correlated.

One strategy to compensate for the low stability of MOFs constructed with large linkers is to increase the connectivity of both organic linkers and inorganic clusters.[7] The Zr_6 cluster $(Zr_6O_4OH_4(COO)_{12})$, which has the highest connectivity among reported zero-dimensional (0-D) inorganic nodes in MOFs, is an outstanding example which endows the framework with excellent stability.[6] In particular, when the linker also exhibits high connectivity, the obtained MOFs are manifested to be robust even with very large pore size.[8] Hence, further increasing the overall connectivity of Zr-MOFs could be an effective strategy allowing construction of highly stable mesoporous MOFs with ultralarge linkers.

Porphyrinic derivatives as organic linkers have been extensively explored in MOFs due to their versatile functionality, such as catalysis, light harvesting, and sensing.[9] Moreover, porphyrinic linkers usually have very large size (∼2 nm), which assists in generating large pores inside the frameworks, resulting in mesoporous MOFs. In order to achieve the high connectivity, we used tetratopic carboxylate

porphyrin ligand H_4TCPP (tetrakis(4-carboxyphenyl)-porphyrin) and the 12-connected Zr_6 cluster to construct mesoporous MOFs. The fully occupied Zr_6 is 12-connected with O_h symmetry, and the free H_4TCPP is four-connected with D_{4h} symmetry (Figure 1). Topological connection of these
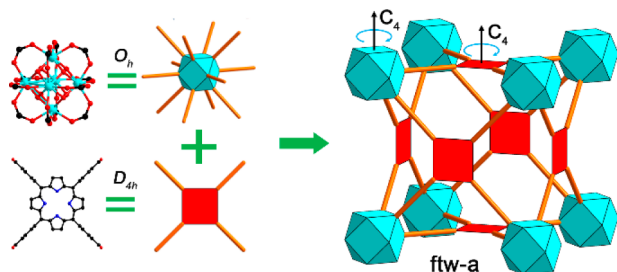

Figure 1. Assembly of O_h and D_{4h} nodes into **ftw-a** network.

two nodes to each other could ideally give rise to a highly connected **ftw-a** network. However, not only the connectivity and symmetry of nodes, but also the direction and relative position of each node, are crucial for topological design, and the latter is often neglected when modulating the building units to obtain the desired structure. In other words, even if both connectivity and symmetry are perfectly matched, it is still not possible to form the expected framework if the relative directions of nodes are not correctly arranged.[10]

Herein, guided by topology and symmetry, porphyrinic linkers (named as H_4TCP-1, H_4TCP-2, and H_4TCP-3) were elongated with desired conformation by arranging the vicinal phenyl ring and carboxylate group. Through combination of the organic linkers and 12-connected Zr_6 cluster, a series of mesoporous MOFs with **ftw-a** topology, namely **PCN-228**, **PCN-229**, and **PCN-230** (PCN stands for porous coordination network), were synthesized. The pore size of these MOFs ranges from 2.5 to 3.8 nm, and **PCN-229** shows both the highest porosity as well as BET surface area among all the previously reported Zr-MOFs. Moreover, the ligand extension does not impair the stability of the material. **PCN-230**, as a representative, which is constructed with the most extended linker, shows excellent stability in aqueous solutions with pH ranging from 0 to 12, demonstrating the highest pH tolerance among all previously reported porphyrinic MOFs.

■ EXPERIMENTAL SECTION

General Information. The commercial chemicals are used as purchased unless otherwise mentioned. Detailed chemical sources are provided in the Supporting Information (SI).

Instrumentation. The powder X-ray diffraction patterns (PXRD) were recorded on a Bruker D8-Focus Bragg−Brentano X-ray Powder diffractometer equipped with a Cu sealed tube ($\lambda = 1.54178$ Å) at room temperature. Synchrotron PXRD measurements were carried out on the beamline 17-BM at the Advanced Photon Source, Argonne National Laboratory, using a wavelength of 0.72775(5) Å and a Perkin-Elmer amorphous-Si Flat Panel Detector. The simulated PXRD spectra were obtained by the diffraction-crystal module of the Mercury program based on the single-crystal data. The program is available free of charge via the Internet at http://www.iucr.org. Thermogravimetric analysis (TGA) was conducted on a TGA-50 (Shimadzu) thermogravimetric analyzer in the air atmosphere. Nuclear magnetic resonance (NMR) data were collected on a Mercury 300 spectrometer. Gas sorption measurements were conducted using a Micrometritics ASAP 2020 system at different temperatures. **PCN-229** or **PCN-230** were activated by supercritical carbon dioxide using MADRIDE prior to gas adsorption.

Synthesis of H_4TCP-1, H_4TCP-2, and H_4TCP-3. Shown in Scheme 1. Details in SI, Section S2.

Scheme 1. Syntheses of H_4TCP-1, -2, and -3 Using the Precursors n_1, n_2, and n_3[a]
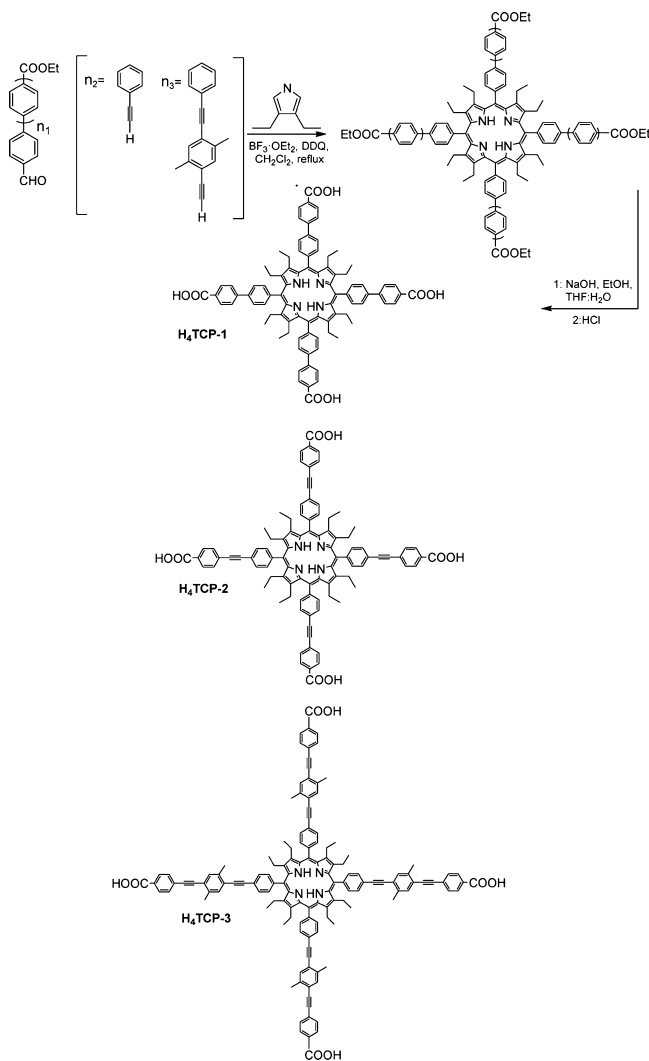
[a]Details of the synthetic procedure are given in the SI.

Synthesis of PCN-228. $(Zr_6(OH)_4O_4(TCP-1)_3 \cdot 10DMF \cdot 2H_2O)$. $ZrCl_4$ (15 mg), H_4TCP-1 (15 mg), and benzoic acid (350 mg) in 2 mL of DMF were ultrasonically dissolved in a 4 mL Pyrex vial. The mixture was heated to 120 °C in an oven for 12 h. After cooling down to room temperature, dark green crystals 16 mg were harvested by filtration (Yield. 85%). Found. C, 67.51; H, 5.63; N, 4.56%.

Synthesis of PCN-229. $(Zr_6(OH)_4O_4(TCP-2)_3 \cdot 45DMF \cdot 25H_2O)$. $ZrCl_4$ (15 mg), H_4TCP-2 1415 (15 mg), and benzoic acid (350 mg) in 2 mL of DMF were ultrasonically dissolved in a 4 mL Pyrex vial. The mixture was heated to 120 °C in an oven for 12 h. After cooling down to room temperature, dark green crystals 14 mg were harvested by filtration (Yield. 82%). Found. C, 56.98; H, 5.95; N, 7.20%.

Synthesis of PCN-230. $(Zr_6(OH)_4O_4(TCP-3)_3 \cdot 30DMF \cdot 10H_2O)$. $ZrCl_4$ (15 mg), H_4TCP-3 (20 mg), and acetic acid (0.4 mL) in 2 mL of DMF were ultrasonically dissolved in a 4 mL Pyrex vial. The mixture was heated to 120 °C in an oven for 24 h. After cooling down to room temperature, dark green crystals 20 mg were harvested by filtration (Yield. 91%). Found. C, 53.83; H, 4.49; N, 2.60%.

Single-Crystal X-ray Crystallography. Single-crystal X-ray crystallographic data of **PCN-228′** and **PCN-230** were collected on a Bruker single-crystal APEXII CCD diffractometer with Mo Kα (λ =

0.71073 Å) at 110 K. All structures were solved by direct methods and refined by full-matrix least-squares on F^2 using SHELXTL.[11] Non-hydrogen atoms were refined with anisotropic displacement parameters during the final cycles. Organic hydrogen atoms were placed in calculated positions with isotropic displacement parameters set to $1.2U_{eq}$ of the attached atom. The solvent molecules are highly disordered, and attempts to locate and refine the solvent peaks were unsuccessful. Contributions to scattering due to these solvent molecules were removed using the SQUEEZE routine of PLATON;[12] structures were then refined again using the data generated. Crystal data were summarized in Table 1. The CIF file can be obtained free of

Table 1. Crystal Data for PCN-228′ and PCN-230

	PCN-228′	PCN-230
formula	$C_{216}H_{120}N_{12}O_{32}Ni_3Zr_6$	$C_{408}H_{318}N_{12}O_{32}Zr_6$
FW	4118.69	6448.06
shape	red square plate	red square plate
crystal system	cubic	cubic
space group	$Pm\overline{3}m$	$Pm\overline{3}m$
a (Å)	25.3468(6)	38.4224(12)
α (deg)	90	90
V (Å^3)	16284.3(7)	56722(3)
Z	1	1
T (K)	110(2)	110(2)
d_{calcd} (g/cm^3)	0.420	0.189
μ(mm^{-1})	0.199	0.037
$F(000)$	2080	3346
θ_{max} (deg)	25.99	23.99
completeness (%)	99.9	99.8
collected reflections	171 630	500 577
unique reflections	3148	8348
parameters	50	66
restraints	29	61
R_{int}	0.0882	0.5735
$R1$ $[I > 2\sigma(I)]$	0.0968	0.1602
$wR2$ $[I > 2\sigma(I)]$	0.2618	0.3489
$R1$ (all data)	0.1023	0.1625
$wR2$ (all data)	0.2683	0.3505
GOF on F^2	1.005	1.004
$\Delta\rho_{max}/\Delta\rho_{min}$ (e·Å^{-3})	2.599/−1.294	1.016/−1.193

charge from the Cambridge Crystallographic Data Centre via www.ccdc.cam.ac.uk/data_request/cif (CCDC 1038049 for **PCN-228′**, 1038050 for **PCN-230**). After the initial structural solution was found on the basis of the single-crystal X-ray diffraction data of **PCN-228′**, the structures of **PCN-228** and **-229** were refined by a self-consistent iterative procedure in which successive geometry optimization calculations were performed using the Forcite module of Materials Studio 6.0.[15] Detailed information about **PCN-228** and **PCN-228′** is present in the SI.

Gas Adsorption of PCN-228, PCN-229, and PCN-230. Before the gas sorption experiment, as-synthesized **PCN-228**(∼100 mg) was washed twice with DMF and acetone, respectively. Fresh acetone was subsequently added, and the sample was allowed to soak for 24 h to exchange and remove the nonvolatile solvates (DMF). After the removal of acetone by decanting, the samples were activated by drying under vacuum, then dried again by using the "outgas" function of the adsorption instrument for 5 h at 100 °C prior to gas adsorption/desorption measurement. For **PCN-229** and **PCN-230**, the as-synthesized samples (∼100 mg) were washed with DMF three times and then soaked in fresh DMF overnight. Afterward, the samples were activated by supercritical CO_2 and then dried again by using the "outgas" function of the adsorption instrument for 5 h at 100 °C prior to gas adsorption/desorption measurement.

Stability Test of PCN-228, -229, and -230. Portions of about 200 mg of as-synthesized samples were separated into several smaller portions and transferred to vials containing aqueous solutions with different pH values. After 24 h, the samples were washed with fresh DMF twice for PXRD measurement (SI, Figures S5−S7) or activated by supercritical CO_2 for N_2 adsorption.

■ RESULTS AND DISCUSSION

Porphyrinic ligands were chosen for reticular chemistry in this work for several reasons. The porphyrin ligand is synthesized from a condensation reaction; elongation of the precursor provides a facile method for the effective enlargement of the target ligands. The elongated porphyrin is relatively easier to synthesize compared with other organic linkers with comparable size. Additionally, the center of a porphyrin is a highly conjugated bulky solid ring, which usually inherently prevents interpenetration. Therefore, using a porphyrinic organic linker could be an effective approach to obtain extra-large pores in MOFs. Moreover, the porphyrin center endows the obtained mesoporous MOFs with versatile functionality which has potential for a wide array of applications. Owing to their large size and the use of relatively soft Lewis acidic metal species as nodes, most reported porphyrinic MOFs suffer from weak stability, which severely hampers their application. Utilizing hard Lewis acidic species as inorganic nodes in porphyrinic MOFs has remarkably improved the chemical stability and extended their use under harsh chemical environments.[8,13]

As shown in Figure 1, the **ftw-a** network is composed of the 12-connected O_h nodes and 4-connected D_{4h} nodes. However, when substituting the corresponding nodes with the 12-connected Zr_6 clusters and TCPP ligands to construct **ftw-a** topology, the peripheral phenyl rings have to rotate into the same plane with the porphyrin. The rotation on position I (Figure 2a) is forbidden because of the steric effect between the porphyrin ring and the phenyl ring. The rotation on position II would destroy the conjugated system between carboxylates and benzene rings, which is also highly energetically nonpreferred. Therefore, these two building units are difficult to form the **ftw-a** network because of their incompatible direction (Figure 2b). The previously reported Zr_6 cluster usually adopts reduced connectivity and symmetry to form other networks with TCPP,[8,13d] or it is fully occupied by TCPP with an energetically disfavored conformation.[13c] Alternatively, the Zr_8 cluster needs to be incorporated with TCPP to construct **ftw-a** network as represented in **PCN-221** (Figure 2d). However, this framework is not stable in aqueous environments because of the charge unbalanced Zr_8 cluster.[13e]

To overcome such conflicts and construct stable mesoporous porphyrinic Zr-MOFs with **ftw-a** topology, the elongated porphyrinic ligands **H₄TCP-1**, **H₄TCP-2**, and **H₄TCP-3** were designed with desired conformation by carefully arranging the vicinal phenyl rings and carboxylate groups. By taking advantage of the steric effect between porphyrin center and connected phenyl rings as well as the adjacent two phenyl rings, the four carboxylate groups in **H₄TCP-1** are likely to stay in the same plane with the porphyrin center which is necessary to form the **ftw-a** network with Zr_6. In contrast, we try to alleviate the steric effect as much as possible for **H₄TCP-2** and **H₄TCP-3**. The ethynyl group is known to promote low or no barrier torsional motion for the vicinal phenyl rings.[14] In **H₄TCP-2** and **H₄TCP-3**, ethynyl moieties were used for ligand elongation, which allow the peripheral benzoates to rotate freely to stay in the same plane as the porphyrin center without significantly increasing the inherent energy. Therefore, the
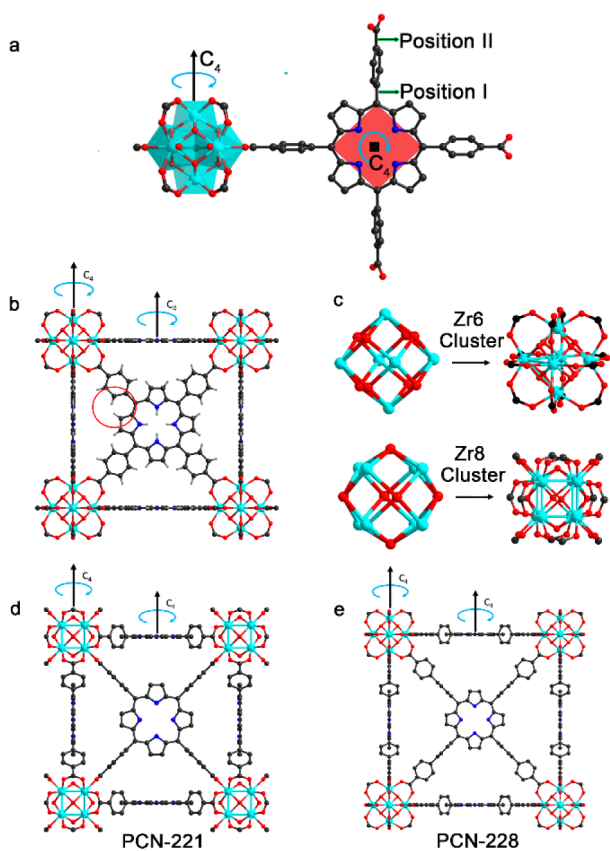
Figure 2. (a) Representation of the connections between the O_h node and D_{4h} node when combining Zr_6 and **H$_4$TCPP**, and the sterically controlled phenyl and carboxylate angle. (b) Substitution of the Zr_6 cluster and **H$_4$TCPP** in **ftw-a** topology and the chemically forbidden conformation of ligand (highlighted with red circle). (c) Representation of the Zr_6 and Zr_8 cluster, and the 90° rotation of the carboxylate groups between these two clusters. (d) Structure of **PCN-221** constructed with Zr_8 cluster and **H$_4$TCPP**. (e) Structure of **PCN-228** constructed with Zr_6 cluster and **H$_4$TCP-1** (ethyl groups were omitted for clarity).

ligands can adopt a compatible direction with the Zr_6 cluster to construct **fta-w** network. Meanwhile, eight ethyl substituents were introduced in the porphyrin rings aiming to increase the solubility of ligands (Scheme 1). Solvothermal reaction of **H$_4$TCP-1**, **H$_4$TCP-2** , or **H$_4$TCP-3** with ZrCl$_4$ and acetic acid in DMF gives rise to large, dark green cubic crystals, namely **PCN-228**, **PCN-229**, and **PCN-230**, respectively (Figure 3a–c). Single-crystal X-ray diffraction reveals a space group of $Pm\overline{3}m$ for **PCN-228′** and **-230** (see SI for details of **PCN-228** and **PCN-228′**). The overall frameworks are based on uniform cubes, each of which has faces consisting of the porphyrinic linker. Although single crystals are also obtained for **PCN-229**, the diffraction is too weak to solve the structure due to their relatively small size. Hence, an isoreticular structure model of **PCN-229** was constructed using Material Studio 6.0,[15] and further confirmed by synchrotron PXRD collected at 17-BM beamline at Advanced Photon Source, Argonne National Laboratory. **PCN-228** and **PCN-230** are also confirmed by the PXRD patterns (Figure 3d). Due to the extra-large size of these porphyrinic linkers, all three MOFs are mesoporous with pore size ranging from 2.5 to 3.8 nm (Figure 3a–c). As we expected, all the peripheral benzoates stay in plane with the porphyrin center, which allows the formation of the **ftw-a**
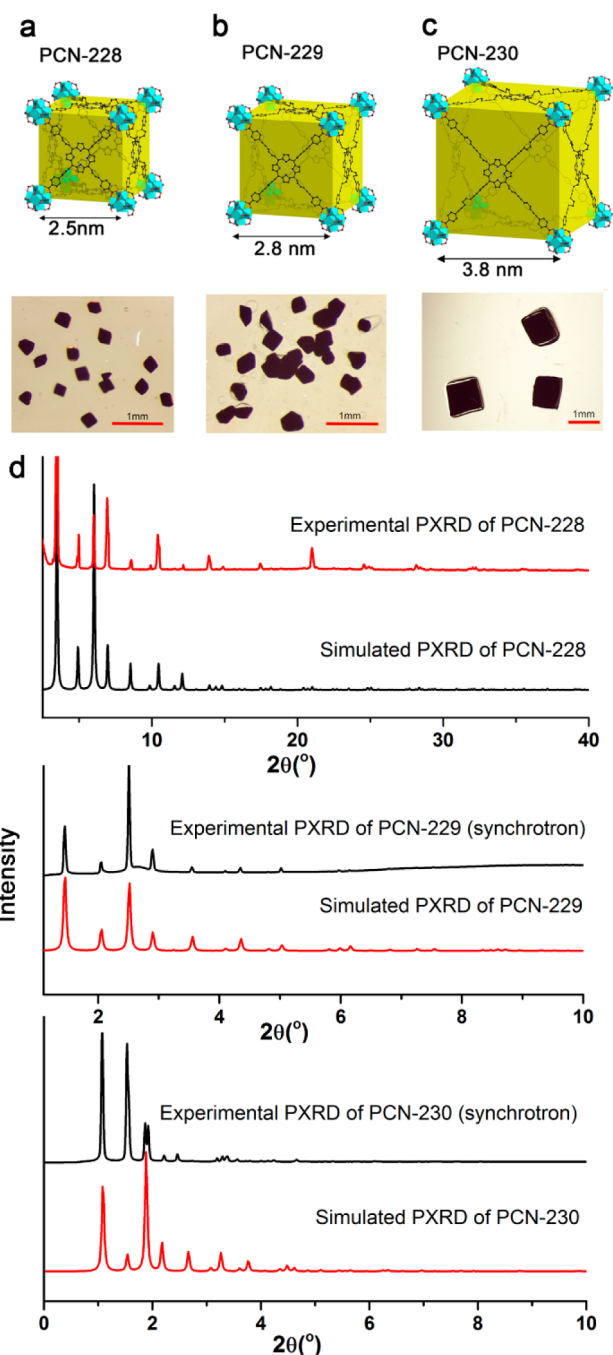

Figure 3. Structures and crystals of (a) **PCN-228**, (b) **PCN-229**, and (c) **PCN-230**. (d) Experimental and simulated PXRD of **PCN-228**, **-229**, and **-230**. (Simulated PXRD of **PCN-228** and **PCN-229** were calculated from the simulated structure.)

network with the 12-connected Zr_6 cluster. Although these MOFs are constructed from Zr_6 clusters, they share the same space group and topology with **PCN-221**, wherein the peripheral benzoates in **TCPP** are perpendicular to the central porphyrin ring. Structural analysis of **PCN-221** has shown the carboxylate groups of the Zr_8 cluster have a 90° rotation compared with that of the Zr_6 cluster (Figure 2c). With this orientation, these two nodes are compatible to form the **ftw-a** topology. However, even with theoretically qualified nodes, some reported zirconium porphyrin MOFs possess reduced connectivity and symmetry due to the incompatible direction-

ality of the metal nodes and linker, resulting in the obtained frameworks with diminished pH stability compared with the 12-connected **PCN-228** series.[5e,8,13c,d] These examples demonstrate that not only the symmetry, but also the relative direction of each node, must be considered in topological MOFs design.

To the best of our knowledge, **PCN-230** exhibits the largest pore among all Zr-MOFs. If we consider Zr-MOF growth as a ligand substitution process taking place with Zr clusters, it is a more entropically favored process when the connecting number on the cluster is higher.[16] Supposing that bond energy of the Zr-carboxylate bond is similar for different connectivity arrangements, the 12-connected porphyrinic Zr-MOFs could be energetically more favored compared to other porphyrinic Zr-MOFs with lower connectivity (it should have a lower Gibbs free energy due to the entropy effect).

In order to assess the porosity of **PCN-228**, **-229**, and **-230**, we performed N_2 sorption measurement at 77 K. **PCN-228**, **PCN-229**, and **PCN-230** show N_2 uptakes of 1245, 1455, and 1085 cm^3/g, respectively (Figure 4a). The experimental Brunauer–Emmett–Teller (BET) surface area is 4510 m^2/g for **PCN-228**, 4619 m^2/g for **PCN-229**, and 4455 m^2/g for **PCN-230**. **PCN-229** shows both the highest porosity and BET surface area among all the previously reported Zr-MOFs as well as among porphyrinic MOFs. The BET surface areas were

calculated to be 4178 m^2/g for **PCN-228**, 4935 m^2/g for **PCN-229** and 7154 m^2/g for **PCN-230** by Materials Studio 6.0 using the "atom volumes and surfaces" function. The inconsistency of experimental and calculated surface area comes from the difficulty in activation of ultrahigh porosity material. The extremely large cavity can easily trap unreacted ligands and metal clusters which are difficult to remove during the activation process. From TGA curves, we can see that the weight loss of **PCN-230** is smaller than that of **PCN-229** after solvent removal at 100 °C (SI, Figure S8). Moreover, **PCN-230** left more residue than **PCN-229** after complete decomposition. This unusual phenomenon supports the idea that PCN-230 may contain bulky trapped species that could not be removed. Moreover, **PCN-230** has the lowest stability among these MOFs, which also accounts for the unexpectedly low N_2 uptake compared with **PCN-228** and **PCN-229**.

Since high volumetric surface area is also crucial for some applications, several highly porous MOFs were selected for comparison of the volumetric and gravimetric surface area and listed in Table 2. The MOFs reported in this work show high gravimetric surface areas. Especially when the volumetric surface area is considered, **PCN-228** is very outstanding among those well-known MOFs. Typically, the MOFs with large pore size possess relative low gravimetric and volumetric surface area. However, **PCN-228** and **PCN-229** possess much higher gravimetric and volumetric surface area compared with **PCN-221** bearing much smaller pore size. The great improvement of both the volumetric and gravimetric surface areas can be ascribed to the replacement of the Zr_8 clusters with the smaller Zr_6 clusters. The low volumetric surface area of **PCN-230** can be ascribed to its extremely low crystal density (0.189 g/cm^3). However, it is still comparable with **PCN-221** which has higher density (0.48 g/cm^3) but much lower gravimetric surface area. Overall, this series of mesoporous MOFs possesses high and permanent porosity after removal of solvent molecules, demonstrating its excellent physical stability.

The Zr_6 cluster is fully occupied by 12 carboxylates from the porphyrinic linkers and gives rise to the highest connectivity among Zr-MOFs, hence this series of MOFs were expected to possess excellent chemical stability. We tested the chemical stability of **PCN-230** as a representative, with consideration that MOF stability decreases along with the increase of the linker length for isoreticular structures. After being soaked in aqueous solutions with pH values ranging from 0 to 12 (prepared with HCl and NaOH solution respectively) for 24 h, the PXRD patterns of **PCN-230** are almost unaltered, which suggests maintenance of the crystallinity (SI, Section S4). To further confirm that the frameworks were intact, we performed N_2 adsorption measurement for samples after different treatments. N_2 uptake measurements of **PCN-230** after treatment have minimal deviation from the pristine sample, which indicates the robustness of the framework under harsh chemical conditions (Figure 4b). To our knowledge, **PCN-230** shows the highest stability in the widest pH range among previously reported porphyrinic MOFs despite its extremely large linker. Stability tests of **PCN-228** and **PCN-229** treated with different aqueous solutions were also conducted (SI, Figures S5 and S6). The well maintained PXRD patterns of the samples after different treatments demonstrate that **PCN-228** and **PCN-229** are stable even in 1 M HCl for 24 h, displaying higher stability than **PCN-230**. This series of Zr-MOFs with elongated linkers successfully realize the combination of meso-
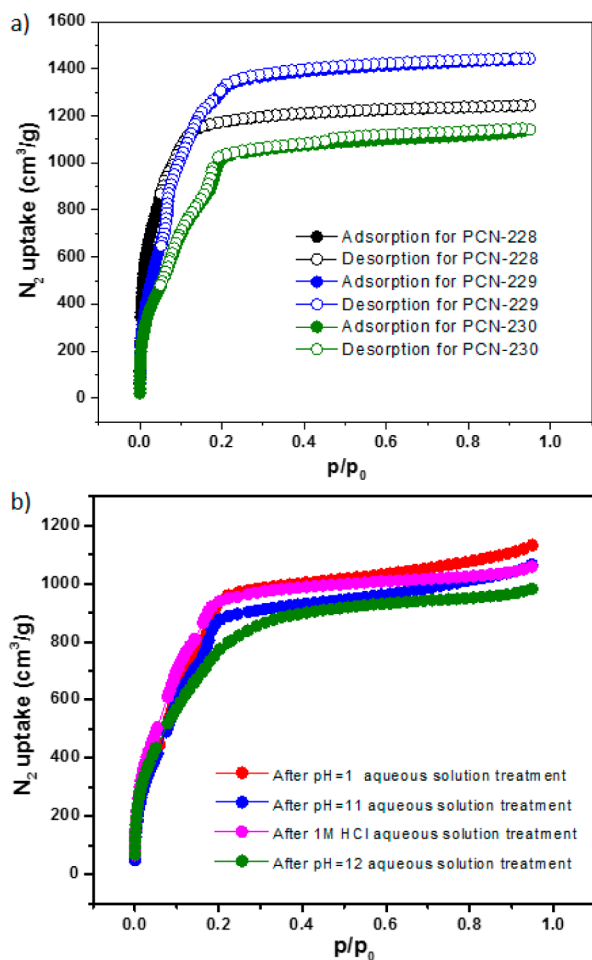

Figure 4. (a) N_2 adsorption isotherms of **PCN-228**, **PCN-229**, and **PCN-230**. (b) N_2 adsorption isotherms of **PCN-230** after different treatment.

Table 2. Volumetric and Gravimetric BET Surface Areas (SA) of Some Highly Porous MOFs

	NU-110E	MOF-210	PCN-610[a]	UMCM-2	NU-111	PCN-229	PCN-228	PCN-230	MIL-101-Cr	MOF-5	PCN-14	MOF-74Mg	PCN-221	HKUST-1
gravimetric SA (m^2/g)	7140	6240	6143	5200	4930	4619	4510	4455	3870	3800	1984	1957	1936	1663
density (g/cm^3)	0.237	0.25	0.303	0.4	0.409	0.32	0.42	0.189	0.44	0.59	0.829	0.909	0.48	0.881
volumetric SA (m^2/cm^3)	1692	1560	1861	2080	2016	1478	1894	842	1702	2242	1644	1779	929	1465
reference	7b	19, 23	7a, 20	18	19	b	b	b	21	17	19	19	13e	22

[a]Also named as NU-100. [b]This work.

porosity with high stability, and would be of great potential for application in nanoscale chemistry.

In conclusion, through topological and symmetry analysis, we developed a series of 12-connected Zr_6 containing porphyrinic MOFs with **ftw-a** topology using elongated porphyrinic linkers. Among them, **PCN-230** exhibits the largest cage (3.8 nm) and **PCN-229** shows both the highest porosity and BET surface area among previously reported Zr-MOFs. **PCN-230**, constructed with the most extended linker, shows excellent stability in aqueous solutions with pH ranging from 0 to 12, the widest range shown by a porphyrinic MOF.

■ ASSOCIATED CONTENT

Ⓢ Supporting Information

Chemicals and instrumentation, full details for sample preparation, characterization results, additional PXRD patterns, and TGA. This material is available free of charge via the Internet at http://pubs.acs.org.

■ AUTHOR INFORMATION

Corresponding Author

zhou@mail.chem.tamu.edu

Author Contributions

§T.-F.L. and D.F. contributed equally to this work.

Notes

The authors declare no competing financial interest.

■ ACKNOWLEDGMENTS

■ REFERENCES

(1) (a) Zhou, H. C.; Long, J. R.; Yaghi, O. M. *Chem. Rev.* **2012**, *112*, 673−674. (b) Zhou, H.-C.; Kitagawa, S. *Chem. Soc. Rev.* **2014**, *43*, 5415−5418.

(2) (a) Zhu, Q.-L.; Xu, Q. *Chem. Soc. Rev.* **2014**, *43*, 5468−5512. (b) Deng, H.; Grunder, S.; Cordova, K. E.; Valente, C.; Furukawa, H.; Hmadeh, M.; Gándara, F.; Whalley, A. C.; Liu, Z.; Asahina, S.; Kazumori, H.; O'Keeffe, M.; Terasaki, O.; Stoddart, J. F.; Yaghi, O. M. *Science* **2012**, *336*, 1018−1023. (c) Hwang, Y. K.; Hong, D. Y.; Chang, J. S.; Jhung, S. H.; Seo, Y. K.; Kim, J.; Vimont, A.; Daturi, M.; Serre, C.; Férey, G. *Angew. Chem., Int. Ed.* **2008**, *47*, 4144−4148. (d) Chen, Y.; Lykourinou, V.; Vetromile, C.; Hoang, T.; Ming, L.-J.; Larsen, R. W.; Ma, S. *J. Am. Chem. Soc.* **2012**, *134*, 13188−13191.

(3) Schaate, A.; Roy, P.; Preuße, T.; Lohmeier, S. J.; Godt, A.; Behrens, P. *Chem.—Eur. J.* **2011**, *17*, 9320−9325.

(4) Pearson, R. G. *J. Am. Chem. Soc.* **1963**, *85*, 3533−3539.

(5) (a) Horcajada, P.; Surblé, S.; Serre, C.; Hong, D.-Y.; Seo, Y.-K.; Chang, J.-S.; Greneche, J.-M.; Margiolaki, I.; Férey, G. *Chem. Commun.* **2007**, 2820−2822. (b) Guillerm, V.; Ragon, F.; Dan-Hardi, M.; Devic, T.; Vishnuvarthan, M.; Campo, B.; Vimont, A.; Clet, G.; Yang, Q.; Maurin, G.; Férey, G.; Vittadini, A.; Gross, S.; Serre, C. *Angew. Chem., Int. Ed.* **2012**, *51*, 9267−9271. (c) Volkringer, C.; Popov, D.; Loiseau, T.; Ferey, G.; Burghammer, M.; Riekel, C.; Haouas, M.; Taulelle, F. *Chem. Mater.* **2009**, *21*, 5695−5697. (d) Lieb, A.; Leclerc, H.; Devic, T.; Serre, C.; Margiolaki, I.; Mahjoubi, F.; Lee, J. S.; Vimont, A.; Daturi, M.; Chang, J.-S. *Microporous Mesoporous Mater.* **2012**, *157*, 18−23. (e) Jiang, H.-L.; Feng, D.; Li, J.-R.; Liu, T.-F.; Zhou, H.-C. *J. Am. Chem. Soc.* **2012**, *134*, 14690−14693. (f) Liu, T. - F.; Zou, L.; Feng, D.; Chen, Y.-P.; Fordham, S.; Wang, X.; Liu, Y.; Zhou, H.-C. *J. Am. Chem. Soc.* **2014**, *136*, 7813−7816. (g) Wei, Z.; Gu, Z.-Y.; Arvapally, R. K.; Chen, Y. − P.; McDougald, R. N., Jr.; Ivy, J. F.; Yakovenko, A. A.; Feng, D.; Omary, M. A.; Zhou, H.- C. *J. Am. Chem. Soc.* **2014**, *136*, 8269−8276. (h) Zhang, M.; Chen, Y.-P.; Bosch, M.; Gentle, T.; Wang, K.; Feng, D.; Wang, Z. U.; Zhou, H.-C. *Angew. Chem., Int. Ed.* **2014**, *53*, 815−818.

(6) (a) Cavka, J. H.; Jakobsen, S.; Olsbye, U.; Guillou, N.; Lamberti, C.; Bordiga, S.; Lillerud, K. P. *J. Am. Chem. Soc.* **2008**, *130*, 13850−13851. (b) Wang, C.; Wang, J.-L.; Lin, W. *J. Am. Chem. Soc.* **2012**, *134*, 19895−19908. (c) Wang, C.; Xie, Z.; deKrafft, K. E.; Lin, W. *J. Am. Chem. Soc.* **2011**, *133*, 13445−13454. (d) Mondloch, J. E.; Bury, W.; Fairen-Jimenez, D.; Kwon, S.; DeMarco, E. J.; Weston, M. H.; Sarjeant, A. A.; Nguyen, S. T.; Stair, P. C.; Snurr, R. Q.; Farha, O. K.; Hupp, J. T. *J. Am. Chem. Soc.* **2013**, *135*, 10294−10297. (e) Furukawa, H.; Gándara, F.; Zhang, Y.-B.; Jiang, J.; Queen, W. L.; Hudson, M. R.; Yaghi, O. M. *J. Am. Chem. Soc.* **2014**, *136*, 4369−4381.

(7) (a) Yuan, D.; Zhao, D.; Sun, D.; Zhou, H. − C. *Angew. Chem., Int. Ed.* **2010**, *49*, 5357−5361. (b) Farha, O. K.; Eryazici, I.; Jeong, N. C.; Hauser, B. G.; Wilmer, C. E.; Sarjeant, A. A.; Snurr, R. Q.; Nguyen, S. T.; Yazaydın, A. Ö.; Hupp, J. T. *J. Am. Chem. Soc.* **2012**, *134*, 15016−15021.

(8) Feng, D.; Gu, Z.-Y.; Li, J.-R.; Jiang, H.-L.; Wei, Z.; Zhou, H.-C. *Angew. Chem., Int. Ed.* **2012**, *51*, 10307−10310.

(9) (a) Zou, C.; Wu, C.-D. *Dalton Trans.* **2012**, *41*, 3879−3888. (b) Burnett, B. J.; Barron, P. M.; Choe, W. *CrystEngComm* **2012**, *14*, 3839−3846. (c) Alkordi, M. H.; Liu, Y.; Larsen, R. W.; Eubank, J. F.; Eddaoudi, M. *J. Am. Chem. Soc.* **2008**, *130*, 12639−12641. (d) Meng, L.; Cheng, Q.; Kim, C.; Gao, W.-Y.; Wojtas, L.; Chen, Y.-S.; Zaworotko, M. J.; Zhang, X. P.; Ma, S. *Angew. Chem., Int. Ed.* **2012**, *51*, 10082−10085. (e) Lee, C. Y.; Farha, O. K.; Hong, B. J.; Sarjeant, A. A.; Nguyen, S. T.; Hupp, J. T. *J. Am. Chem. Soc.* **2011**, *133*, 15858−15861. (f) Son, H.-J.; Jin, S.; Patwardhan, S.; Wezenberg, S. J.; Jeong, N. C.; So, M.; Wilmer, C. E.; Sarjeant, A. A.; Schatz, G. C.; Snurr, R. Q.; Farha, O. K.; Wiederrecht, G. P.; Hupp, J. T. *J. Am. Chem. Soc.* **2013**, *135*, 862−869. (g) Gao, W.-Y.; Chrzanowski, M.; Ma, S. *Chem. Soc. Rev.* **2014**, *43*, 5841−5866. (h) Park, J.; Feng, D.; Yuan, S.; Zhou, H.-C. *Angew. Chem., Int. Ed.* **2014**, DOI: 10.1002/anie.201408862.

(10) Li, M.; Li, D.; O'Keeffe, M.; Yaghi, O. M. *Chem. Rev.* **2014**, *114*, 1343−1370.

(11) Sheldrick, G. *Acta Crystallogr. A* **2008**, *64*, 112−122.

(12) Spek, A. *J. Appl. Crystallogr.* **2003**, *36*, 7.

(13) (a) Fateeva, A.; Chater, P. A.; Ireland, C. P.; Tahir, A. A.; Khimyak, Y. Z.; Wiper, P. V.; Darwent, J. R.; Rosseinsky, M. J. *Angew. Chem., Int. Ed.* **2012**, *51*, 7440−7444. (b) Chen, Y.; Hoang, T.; Ma, S. *Inorg. Chem.* **2012**, *51*, 12600−12602. (c) Morris, W.; Volosskiy, B.; Demir, S.; Gándara, F.; McGrier, P. L.; Furukawa, H.; Cascio, D.; Stoddart, J. F.; Yaghi, O. M. *Inorg. Chem.* **2012**, *51*, 6443−6445. (d) Feng, D.; Chung, W.-C.; Wei, Z.; Gu, Z.-Y.; Jiang, H.-L.; Chen, Y.-P.; Darensbourg, D.; Zhou, H.-C. *J. Am. Chem. Soc.* **2013**, *135*, 17105−17110. (e) Feng, D.; Jiang, H.-L.; Chen, Y.−P.; Gu, Z.-Y.; Wei, Z.; Zhou, H.-C. *Inorg. Chem.* **2013**, *52*, 12661−12667. (f) Feng, D.; Gu, Z.-Y.; Chen, Y.-P.; Park, J.; Wei, Z.; Sun, Y.; Bosch, M.; Yuan, S.; Zhou, H.-C. *J. Am. Chem. Soc.* **2014**, *136*, 17714−17717.

(14) Okuyama, K.; Hasegawa, T.; Ito, M.; Mikami, N. *J. Phys. Chem.* **1984**, *88*, 1711−1716.

(15) *Accelrys Materials Studio Release Notes*, Release 5.5.1; Accelrys Software, Inc.: San Diego, 2010.

(16) Feng, D.; Wang, K.; Wei, Z.; Chen, Y.-P.; Simon, C. M.; Arvapally, R. K.; Martin, R. L.; Bosch, M.; Liu, T.-F.; Fordham, S.; Yuan, D.; Omary, M. A.; Haranczyk, M.; Smit, B.; Zhou, H.-C. *Nature Commun.* **2014**, *5*, No. 5723.

(17) Kaye, S. S.; Dailly, A.; Yaghi, O. M.; Long, J. R. *J. Am. Chem. Soc.* **2007**, *129*, 14176−14177.

(18) Koh, K.; Wong-Foy, A. G.; Matzger, A. J. *J. Am. Chem. Soc.* **2009**, *131*, 4184−4185.

(19) Mason, J. A.; Veenstrab, M.; Long, J. R. *Chem. Sci.* **2014**, *5*, 32−51.

(20) Farha, O. K.; Yazaydın, A. Ö.; Eryazici, I.; Malliakas, C. D.; Hauser, B. G.; Kanatzidis, M. G.; Nguyen, S. T.; Snurr, R. Q.; Hupp, J. T. *Nature Chem.* **2010**, *2*, 944−948.

(21) Wiersum, A. D.; Chang, J.-S.; Serre, C.; Llewellyn, P. L. *Langmuir* **2013**, *29*, 3301−3309.

(22) Chowdhury, P.; Mekala, S.; Dreisbach, F.; Gumma, S. *Microporous Mesoporous Mater.* **2012**, *152*, 246−252.

(23) Furukawa, H.; Ko, N.; Go, Y. B.; Aratani, N.; Choi, S. B.; Choi, E.; A. Yazaydin, Ö.; Snurr, R. Q.; O'Keeffe, M.; Kim, J.; Yaghi, O. M. *Science* **2010**, *329*, 424−428.